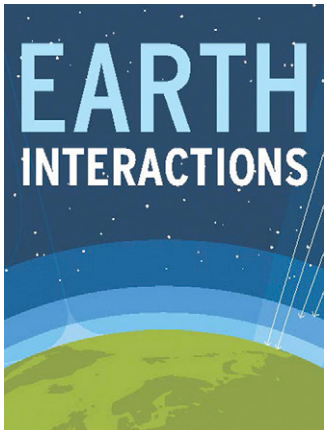

The Impacts of Land-Use and Land-Cover Change on Tropospheric Temperatures at Global and Regional Scales

Weiyue Zhang

Institute for Climate and Global Change Research and School of Atmospheric Sciences, Nanjing University, and Jiangsu Collaborative Innovation Center for Climate Change, Nanjing, China

Zhongfeng Xu*

Key Laboratory of Regional Climate-Environment for Temperate East Asia, Institute of Atmospheric Physics, Chinese Academy of Sciences, Beijing, and Jiangsu Collaborative Innovation Center for Climate Change, Nanjing, China

Weidong Guo

Institute for Climate and Global Change Research and School of Atmospheric Sciences, Nanjing University, and Jiangsu Collaborative Innovation Center for Climate Change, Nanjing, China

Received 14 May 2015; in final form 27 October 2015

* Corresponding author address: Dr. Zhongfeng Xu, 40 Hua Yan Li, Qi Jia Huo Zi, Institute of Atmospheric Physics, Chinese Academy of Sciences, Beijing 100029, China.
E-mail address: xuzhf@tea.ac.cn

DOI: 10.1175/EI-D-15-0029.1

ABSTRACT: The impacts of land-use and land-cover change (LULCC) on tropospheric temperatures are investigated in this study using the fully coupled Community Earth System Model. Two simulations are performed using potential and current vegetation cover. The results show that LULCC can induce detectable changes in the tropospheric air temperature. Although the influence of LULCC on tropospheric temperature is weak, a significant influence can still be found below 300 hPa in summer over land. Compared to the global-mean temperature change, LULCC-induced changes in the regional-mean air temperature can be 2–3 times larger in the middle–upper troposphere and approximately 8 times larger in the lower troposphere. In East Asia and South Asia, LULCC is shown to produce significant decreases (0.2° to 0.4°C) in air temperature in the middle–upper troposphere in spring and autumn due to the largest decrease in the latent heat release from precipitation. In Europe and North America, the most significant tropospheric cooling occurs in summer, which can be attributed to the significant decrease in the absorbed solar radiation and sensible heat flux during this season. In addition to local effects, LULCC also induces nonlocal responses in the tropospheric air temperature that are characterized by significant decreases over the leeward sides of LULCC regions, which include East Asia–western North Pacific Ocean, Mediterranean Sea–North Africa, North America–Atlantic Ocean, and North America–eastern Pacific. Cooling in the leeward sides of LULCC regions is primarily caused by an enhanced cold advection induced by LULCC.

KEYWORDS: Air temperatures; Seasonality; Nonlocal response; Temperature advection

1. Introduction

Human activities have altered 42%–68% of the global land surface by transforming natural vegetation into crops, pastures, and woods for harvesting from the years 1700 to 2000 (Hurtt et al. 2006). The biogeophysical climate impacts of human-induced land-cover change have been investigated using various general circulation models (GCM), regional climate models, and observations (e.g., Pielke et al. 2002; Fu 2003; Feddema et al. 2005; Bonan 2008). The Fifth Assessment Report of the Intergovernmental Panel on Climate Change (IPCC; Myhre et al. 2013) noted that global land-use change has led to a change in radiative forcing by $-0.15 \pm 0.10\,\mathrm{W\,m^{-2}}$ due to the increased land surface albedo, which in turn caused a decrease in the land surface temperature (LST). However, the nonradiative influence of land-use change [e.g., changes in plant phenology and evapotranspiration (ET)] led to an increase in the LST because of the decrease in ET (Pitman et al. 2009; Lawrence and Chase 2010).

The influence of land-use and land-cover change (LULCC) on the LST is different at different latitudes. In tropical and temperate regions (e.g., South Asia and East Asia), LULCC can lead to a surface warming of 1° to 2°C via reduced evapotranspiration (Shukla et al. 1990; Dickinson and Kennedy 1992; Polcher and Laval 1994; Zhang et al. 1996; Chase et al. 1996; Pielke 2001; Niyogi et al. 2002; Davin and de Noblet-Ducoudré 2010). In high-latitude regions, such as Europe and North America, LULCC can result in a surface temperature cooling of 1° to 2°C primarily because of the increased land surface albedo (Brovkin et al. 1999; Betts et al. 2007; Oleson et al. 2004; Bala et al. 2007; Davin and de Noblet-Ducoudré

2010; de Noblet-Ducoudré et al. 2012). Lawrence and Chase (2010) found that land-cover change results in a widespread regional warming and drying of the near-surface atmosphere but has a limited global influence on near-surface temperatures and precipitation. The LULCC-induced warming is significantly driven by changes in surface hydrology due to reduced ET, while radiative forcing plays a secondary role (Lawrence and Chase 2010).

Most previous studies focused on the influence of LULCC on the surface air temperature, precipitation, and land–atmosphere fluxes (e.g., Brovkin et al. 1999; Betts et al. 2007; Oleson et al. 2004; Douglas et al. 2006; Lobell et al. 2006; Bala et al. 2007; Lee et al. 2009). Only a few studies have investigated the potential impact of LULCC on the troposphere. For example, a GCM simulation with a prescribed SST suggested that the impacts of terrestrial quantities (e.g., soil moisture and sensible and latent heat fluxes) resulting from LULCC over South Asia and Southeast Asia can rarely propagate into the atmosphere in a significant way in summer (Findell et al. 2009). However, Narisma and Pitman (2003) investigated the influence of LULCC on regional climates using an RCM and noted that LULCC has the potential to influence atmospheric circulation patterns over Australia as well as the boundary layer temperature. In their simulations, the influence of LULCC on temperature propagates upward beyond the boundary layer and reached a height of approximately 0.7-sigma level (Narisma and Pitman 2003). A recent study using a fully coupled Community Earth System Model (CESM) showed that LULCC could significantly affect atmospheric circulation at 850 hPa in Asia during the monsoon seasons of spring and autumn (Xu et al. 2015). Given the diverse results of the influence on the troposphere caused by LULCC, we revisit this issue by investigating the influence of LULCC on tropospheric air temperatures using a fully coupled Earth system model in this study.

In addition to studies of the local climatic responses to LULCC, the remote climate response to LULCC has also been investigated in previous studies. For example, the land-cover change in the tropics and Southeast Asia could affect climate at higher latitudes by changing the position and strength of the Hadley and Walker circulations (Zhao et al. 2001). A GCM simulation suggested that tropical deforestation causes a weakening of deep tropical convection, which triggers the northeastward propagation of a Rossby wave train and alters climates at higher latitudes (Snyder 2010). A coupled ocean–atmosphere model simulation showed that Southeast Asian deforestation can also induce teleconnections between the tropics and the extratropics via the excitation of atmospheric waves (Schneck and Mosbrugger 2011). Schneck and Mosbrugger (2011) also noted that remote effects are sensitive to small initial changes, which suggests that the remote responses to land-cover change contain high uncertainties. Findell et al. (2006) argued that the extratropical response to complete tropical deforestation is difficult to distinguish from natural climate variability. In this study, we further investigate the influence of LULCC on tropospheric air temperatures and its nonlocal effects, which have not been investigated thoroughly in previous studies.

This paper is organized as follows: The model description and experimental design are outlined in section 2. Section 3 presents the influence of LULCC on surface temperatures. Changes in the 850-hPa air temperature, the nonlocal responses of air temperatures to LULCC, and the change in the vertical profile of air temperatures are addressed in section 4. Conclusions are last presented in section 5.

2. Model introduction and experimental design

2.1. Model

This study uses the CESM developed by the National Center for Atmospheric Research (NCAR) (Collins et al. 2006). The CESM is a fully coupled Earth system model that includes four separate model components that can simultaneously simulate Earth's atmosphere, ocean, land surface, and sea ice physics. The atmosphere component of the CESM is the Community Atmosphere Model (CAM), which uses a Lin–Rood finite-volume dynamic core. The horizontal resolution of the CAM in this study is 2.5° × 1.875° with 26 levels in the vertical direction (Lin 2004). The ocean model used in this study is version 2 of the Parallel Ocean Program, which can simulate dynamic and thermodynamic processes in the ocean (Smith et al. 2010). The land surface component of the CESM is the Community Land Model, version 4 (CLM4), which is able to simulate biophysical, biochemical, and hydrological processes. Land-cover types in the CLM include 15 vegetation types in addition to bare ground, lake, and glacier. Each vegetation type has its own leaf area and stem area indices, root distribution, optical properties, and canopy heights at its top and bottom (Dai et al. 2003). The improvements in the CLM4 compared to its previous version include a refinement of the global plant function type (PFT), a better description of wetland and lake distributions, and more realistic optical properties for grasslands and croplands. In particular, more sophisticated representations of soil hydrology and snow processes are implemented in the CLM4. The sea ice component of the CESM, which is called the Community Ice Code (CICE), is a dynamic–thermodynamic model that includes a subgrid-scale ice thickness distribution (Bitz et al. 2001; Lipscomb 2001).

Like its predecessors, the current CESM can reasonably reproduce the annual cycle of precipitation and temperature and diurnal temperature variation (e.g., Meehl et al. 2006; Xu et al. 2015). However, significant errors have also been noted; for example, CCSM3 exhibits systematic SST errors that are associated with regional precipitation errors in the monsoon regions of South America and West Africa, although the coupled model showed some improvements in the monsoon simulation compared to the SST-forced simulations, particularly for Asia (Meehl et al. 2006). CCSM4 contains significant improvements compared to CCSM3, including a smaller systematic rainfall error, a more realistic pattern of rainfall in the Australian monsoon, and an improved simulation of El Niño (Meehl et al. 2012). The comparison of the CESM simulation, which is driven by realistic external forcings of greenhouse gas concentration, anthropogenic aerosol, and land-cover change, with the NCEP–NCAR reanalysis shows a warmer temperature bias in the annual mean of 850-hPa air temperature in most regions from the years 1979 to 2005. The CESM results show significant temperature biases (i.e., larger than 4°C) at the North and South Poles, on the Tibetan Plateau, and over the southeastern Pacific Ocean. Conversely, the biases are generally less than 4°C in East Asia, South Asia, Europe, and North America (figure not shown). The vertical profile of the simulated annual-mean air temperature also shows a warm bias of approximately 1°C below 300 hPa over East and South Asia and a bias of approximately 1° to 4°C in Europe and North America. The maximum bias occurs in the lower troposphere (figure not shown).

2.2. Experimental design

To investigate possible influences of LULCC on tropospheric air temperature, two experiments are conducted using the fully coupled CESM. The experiments are the same as employed in Xu et al. (2015), and the following text is derived from there with minor modifications. In the first experiment (i.e., PotVeg), we use potential vegetation cover data that is available in the literature (Ramankutty and Foley 1999; Lawrence and Chase 2010). This dataset was originally derived primarily from a satellite-based global land-cover dataset with regions dominated by land use filled using a simulated potential vegetation dataset from an equilibrium terrestrial biosphere model (Haxeltine and Prentice 1996). The second experiment (i.e., CurVeg) is driven by current vegetation cover data valid in 2000 from Moderate Resolution Imaging Spectroradiometer (MODIS) data. Both experiments were run for 100 years. Both the CAM and CLM were initialized from the current climatological-mean state of 1 January. Present-day oceanic temperature and salinity were used to initialize the ocean model. It is necessary to have the upper ocean reach a reasonable state of equilibrium to investigate interannual climate variability (Kantha and Clayson 2000). In our simulations, the annual-mean SST takes approximately 10 to 20 years to reach equilibrium, which is generally consistent with previous studies (Abe et al. 2003; Wohlfahrt et al. 2004; Kitoh 2004). Deep soil moisture requires approximately 30 years to be in a reasonable state of equilibrium. Therefore, in order to exclude spinup effects, the first 40 years of the simulations were discarded from the subsequent analysis. The climatological-mean difference between the CurVeg and PotVeg experiments (i.e., CurVeg minus PotVeg) describes the effects of LULCC.

LULCC led to significant changes in tree, crop, shrub, and grass PFTs between the current and potential vegetation covers considered (Figure 1). Tree PFTs show the largest decrease in East Asia, South Asia, central Europe, and North America, which is consistent with that in Lawrence and Chase (2010). In these regions, the decreased tree PFTs are primarily converted into crop and grass PFTs. Figure 2 shows the changes in the leaf area index (LAI), the surface albedo, and the effective roughness length between the current and potential vegetation covers. Following Maynard and Royer (2004), the effective roughness length Z_0^e is computed by

$$\frac{1}{\left[\ln\left(\frac{Z_b}{Z_0^e}\right)\right]^2} = \sum_i f_i \frac{1}{\left[\ln\left(\frac{Z_b}{Z_0^i}\right)\right]^2}, \tag{1}$$

where f_i is the fractional area of each land-use category i, Z_0^i is the roughness length, and Z_b is the height of the first atmospheric model level above the ground (i.e., 65 m). Although Z_b varies with orography to a certain extent, the effective roughness length shows a very low sensitivity to the change in Z_b.

Generally, the LAI and effective roughness length show a significant decrease in East Asia, South Asia, central Europe, and North America due to anthropogenic LULCC (Figures 2a,c). Conversely, surface albedo shows a significant increase in these regions (Figure 2b). The decrease in the LAI is larger in East Asia and South Asia than that in Europe and North America (Table 1). Conversely, the changes in

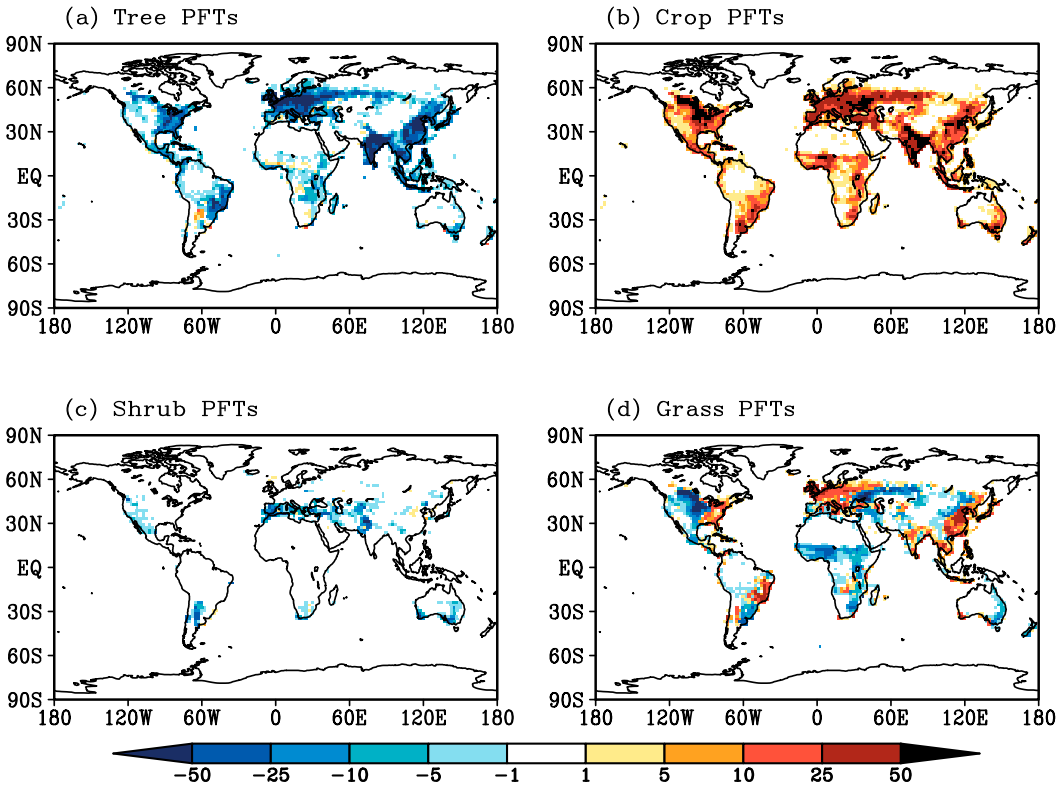

Figure 1. Land-cover change in the CLM plant functional types (PFTs; unit: %) between the current day and the potential vegetation parameters (i.e., CurVeg minus PotVeg).

surface albedo and effective roughness length in East Asia and Europe are larger than in South Asia and North America throughout the year (Table 2).

3. Impact of LULCC on the land surface temperature

For comparison, the response of the LST to LULCC is investigated (Figure 3) prior to the response of tropospheric temperature to LULCC. The Student's t test, which takes serial correlation into account, is used to identify the statistically significant differences between the results of these two experiments (Zwiers and von Storch 1995). It is found that LULCC produces a significant increase of 1° to 3°C in the LST over South Asia and East Asia throughout the year (Figure 3). LULCC leads to a significant decrease in the LST in North America and North Africa throughout the year except in spring (Figure 3). LULCC-induced changes in the 2-m air temperature are generally consistent with those in the LST in all seasons (not shown). It is worth noting that LULCC can also lead to some nonlocal responses in the LST (Figure 3), which will be described in section 4.2.

Following Xu et al. (2015), we compute each individual term that contributes to the land surface energy balance:

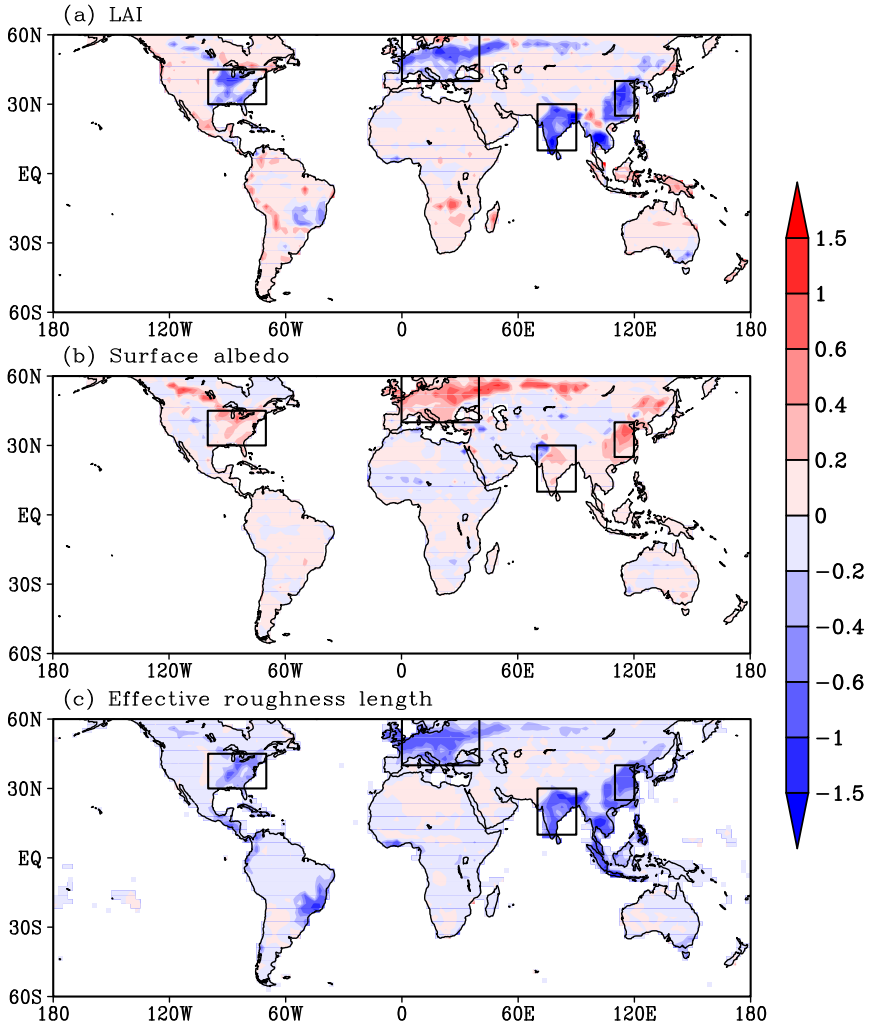

Figure 2. Differences in (a) annual-mean LAI, (b) land surface albedo ($\times 10^{-1}$), and (c) effective roughness length (unit: m) between the CurVeg and PotVeg experiments (i.e., CurVeg minus PotVeg). The four regions are outlined by black boxes.

$$R_a - (L_\uparrow - L_\downarrow) - H - \lambda E - G = 0. \tag{2}$$

The longwave radiation emitted from the land surface can be written as

$$\sigma T^4 = R_a + L_\downarrow - H - \lambda E - G, \tag{3}$$

where σ is the Stefan–Boltzmann constant, which equals $5.67 \times 10^{-8}\,\mathrm{W\,m^{-2}\,K^{-4}}$; T is the land surface temperature (i.e., the radiative temperature); R_a is the absorbed solar radiation (ASR) at the land surface; $L_\uparrow$ is the emitted longwave radiation from the land surface; $L_\downarrow$ is the atmospheric longwave radiation (ALR); H is the sensible heat (SH) flux; λE is the latent heat (LH) flux; and G is the ground

Table 1. Difference in LAI between CurVeg and PotVeg experiments (i.e., CurVeg minus PotVeg). East Asia: 25°–40°N, 110°–120°E; South Asia: 10°–30°N, 70°–90°E; Europe: 40°–60°N, 0°–40°E; and North America: 30°–45°N, 70°–100°W.

	Spring	Summer	Autumn	Winter	Annual
East Asia	−0.58	−0.79	−0.64	−0.48	−0.62
South Asia	−0.48	−0.53	−0.78	−0.73	−0.63
Europe	−0.15	−0.36	−0.27	−0.18	−0.24
North America	−0.28	−0.40	−0.26	−0.09	−0.26
Global mean	0.00	−0.01	−0.01	−0.01	−0.01

heat flux (GHF). Thus, we can determine which components of the surface energy budget are responsible for the change of the land surface temperature by analyzing the changes in the land surface fluxes.

Figure 4 shows the LULCC-induced changes in each component of the surface energy budget in five regions. The GHF, SH, and LH have been multiplied by −1, respectively, for comparison. Thus, a positive (negative) change favors the warming (cooling) of the land surface, as shown in Equation (3). The total positive (negative) changes are larger than the total negative (positive) changes in East Asia and South Asia (Europe, North America, and North Africa), indicating a warming (cooling) of the land surfaces in these regions (Figure 4). In East Asia, LULCC leads to an increase in the seasonal-mean LST due to the significantly lower SH throughout the year except in winter, although ASR decreases due to the increase in surface albedo (Figures 3, 4a). The reduced LH accounts for the significant increase in the LST in South Asia throughout the year (Figures 3, 4b). In Europe and North America, ASR decreases due to the increase in surface albedo, which favors the land surface cooling. However, the significant decrease in SH tends to warm the land surface, which largely cancels out the cooling effect induced by albedo change (Figures 4c,d). As a result, the cooling is weak in Europe and North America (Figure 3). There is a significant cooling in North Africa due to the decreased ALR and the increased SH throughout the year except in spring, although LULCC is not significant here (Figures 3, 4e). The mechanism of the change in ALR and SH will be discussed in section 4.2.

4. Impact of LULCC on the upper air temperature

4.1. Changes in the 850-hPa air temperature

The influence of LULCC on the 850-hPa air temperature is different from that on the LST. The air temperature shows an overall cooling at 850 hPa over LULCC regions, including India and eastern China, where LULCC leads to a land surface

Table 2. Difference in land surface albedos between CurVeg and PotVeg experiments (i.e., CurVeg minus PotVeg). Regional areas defined in Table 1.

	Spring	Summer	Autumn	Winter	Annual
East Asia	0.028	0.022	0.037	0.045	0.033
South Asia	0.017	0.007	0.005	0.010	0.010
Europe	0.021	0.015	0.028	0.037	0.026
North America	0.013	0.007	0.016	0.030	0.016
Global mean	0.003	0.001	0.003	0.005	0.003

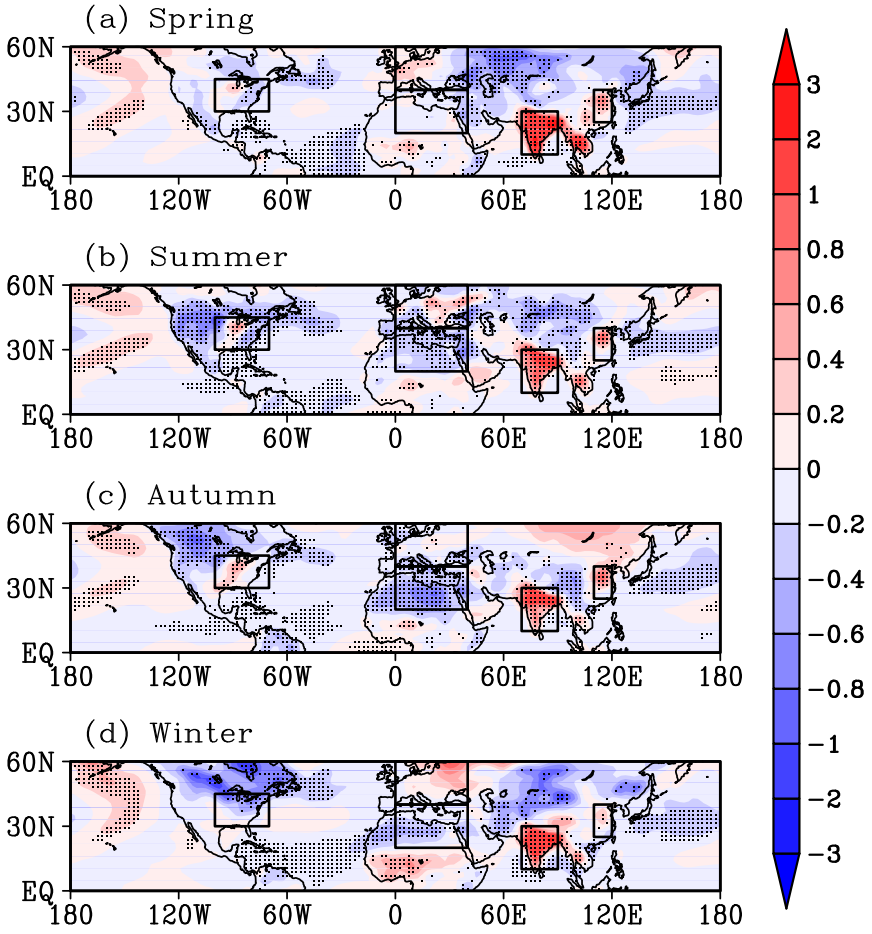

Figure 3. LULCC-induced changes in surface temperature in (a) spring (March–May), (b) summer (June–August), (c) autumn (September–November), and (d) winter (December–February). The sitppled area denotes that the difference reaches the significance level of 0.05. The four regions are indicated by black boxes.

warming (Figures 3, 5). LULCC induces a significant decrease in the 850-hPa air temperature in East Asia, Europe, and North America in spring, summer, and autumn (Figure 5), but the influence of LULCC is less significant in winter in Europe and North America (Figure 5d). As discussed in section 3, LULCC leads to distinct decreases in the surface roughness, sensible heat flux, and latent heat flux from evaporation (Figures 2c, 4), which generally tend to warm the land surface and cool the atmosphere. Conversely, LULCC-induced increases in the land surface albedo tend to reduce the energy absorbed by the land and results in surface cooling (Figure 2b). In addition, the model results indicate that the atmospheric precipitable water also decreases in response to LULCC, which is favorable for the decrease in tropospheric air temperatures due to the reduced greenhouse gas effect of water vapor in the atmosphere (Xu et al. 2015). Consequently, LULCC results in an overall decrease in 850-hPa air temperatures in Europe, East Asia, North

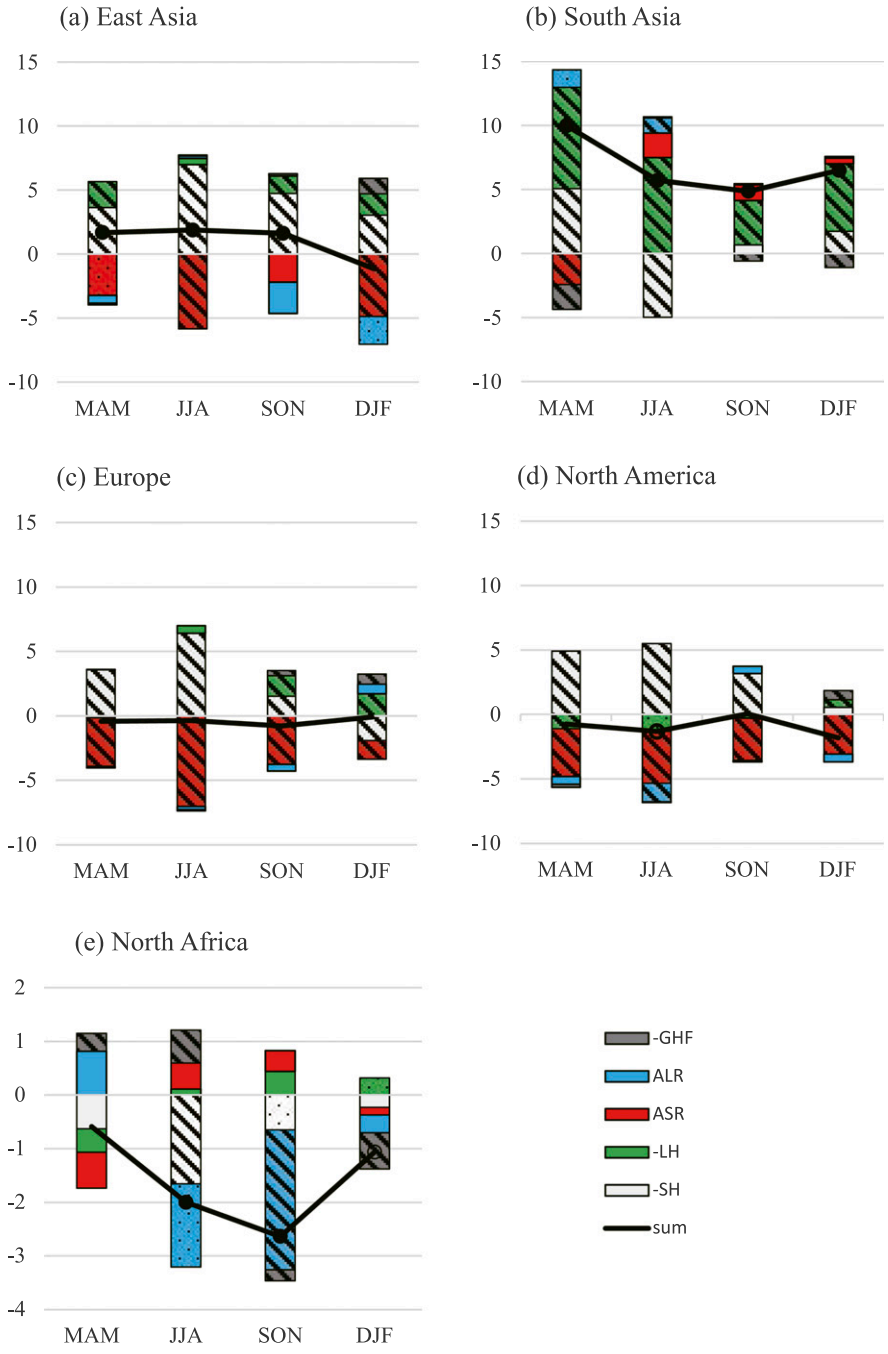

Figure 4. LULCC-induced changes in seasonal-mean fluxes ($W m^{-2}$) in (a) East Asia (25°–40°N, 110°–120°E), (b) South Asia (10°–30°N, 70°–90°E), (c) Europe (40°–60°N, 0°–40°E), (d) North America (30°–45°N, 70°–100°W), and (e) North Africa (20°–40°N, 0°–40°E). GHF, SH, LH, ASR, ALR, and the sum of the five variables. GHF, SH, and LH have been multiplied by −1, respectively, for comparison. A positive (negative) change tends to warm up (cool down) the land surface. The hatched (stippled) bars indicate that the differences reach the significance level of 0.05 (0.10). The solid (open) circle indicates the difference in the sum reaches the significance level of 0.05 (0.10), respectively.

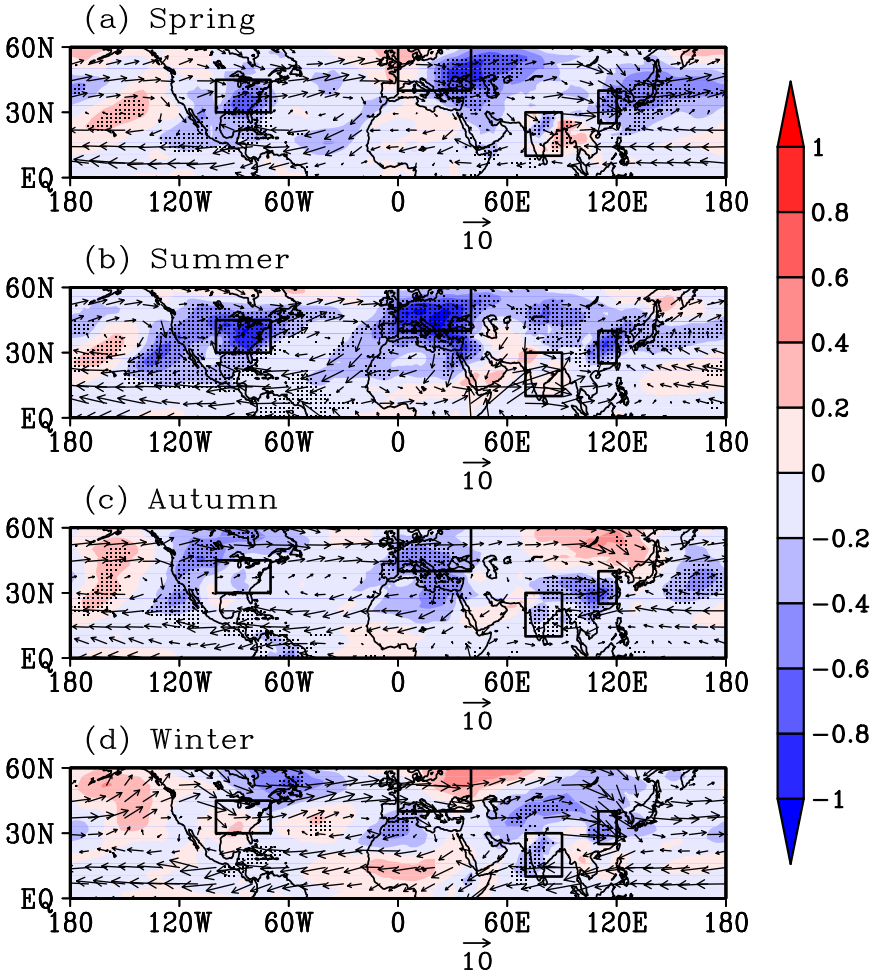

Figure 5. LULCC-induced changes in 850-hPa air temperature in (a) spring (March–May), (b) summer (June–August), (c) autumn (September–November), and (d) winter (December–February). The stippled area denotes that the difference reaches the significance level of 0.05. The four regions are indicated by black boxes. The vector is the climatological wind in the CurVeg experiment at 850 hPa.

America, and the adjacent ocean areas (Figure 5). Conversely, changes in the LST are determined by the relative importance of the two factors that have opposing effects on the LST change: LULCC-induced increases in the land surface albedo tend to cool the land surface, while decreases in the land surface roughness, sensible heat, and latent heat fluxes tend to warm the land surface.

4.2. Nonlocal responses of air temperature to LULCC

In addition to local responses, we also found significant nonlocal responses of tropospheric air temperatures to LULCC (Figure 5). The 850-hPa air temperature

shows a significant decrease over the leeward side of LULCC regions (e.g., East Asia to the western North Pacific Ocean, the Mediterranean Sea to North Africa, North America to the Atlantic Ocean, and North America to the eastern Pacific Ocean; see Figure 5). Similar to the local responses, the nonlocal responses to LULCC are also season dependent (Figure 5). In East Asia, the significant cooling at 850 hPa extends to the western North Pacific in spring and summer, which is likely related to the enhanced cold advection from eastern China to the western North Pacific caused by westerly wind (Figures 5a,b). In autumn, significant cooling is constrained to the East Asian continent, where a convergent zone of 850-hPa wind exists (Figure 5c). Thus, LULCC-induced cooling cannot effectively propagate to the western North Pacific in autumn. In winter, the change in the 850-hPa air temperature is weak in the East Asia continent. Thus, no significant change is found in 850-hPa air temperatures in the western North Pacific in winter, even though the westerly winds in this region are strong (Figure 5d). In the western North Pacific, the most significant cooling occurs in spring and is characterized by a 0.4°–0.6°C decrease in 850-hPa air temperatures (Figure 5a). The area with a significant decrease in air temperature tilts eastward and extends to 165°E at 500 hPa in spring (Figure 6a).

In Europe, LULCC-induced cooling is brought to the Mediterranean Sea and North Africa by a northerly wind, leading to a significant decrease in 850-hPa air temperatures in this region in summer and autumn (Figures 5b,c). In summer, the decrease in 850-hPa air temperatures can reach up to 0.4°C in North Africa (Figure 5b). The decrease in 850-hPa air temperature leads to a significant increase in the temperature gradient between land surface and low-level atmosphere, which in turn causes a significant increase in SH (Figure 4e). On the other hand, the decrease in 850-hPa air temperature causes a significant decrease in ALR in North Africa (Figure 4e). Both the decrease in ALR and increase in SH favor the land surface cooling in North Africa (Figures 4e, 3). In North America, LULCC-induced cooling propagates to the North Atlantic Ocean by the advection of southwesterly winds and to the eastern Pacific Ocean by the advection of northeasterly winds. In summer, the 850-hPa air temperature shows the strongest local and nonlocal responses to LULCC. A significant cooling of 0.6°–0.8°C is found in the northwest Atlantic Ocean and eastern Pacific Ocean in summer. The cooling in summer is the strongest compared to that in other seasons (Figure 5).

The significant cooling tilts westward with an increase in height in East Asian, western North Pacific Ocean, North American, and North Atlantic Ocean regions, where westerly winds prevail. It appears that ascending motion helps to propagate significant cooling to the upper troposphere (Figures 6a,c). Conversely, cooling is limited to the middle and lower troposphere in the eastern Pacific Ocean, where descending motions dominate (Figure 6d). The 850-hPa air temperature significantly decreases by 0.4°–0.6°C in the eastern Pacific Ocean region in summer, and cooling can extend to 140°W (Figures 5b, 6d).

As shown in Figure 7, the LULCC-induced changes in the 850-hPa air temperatures show a good linear relationship with the LULCC-induced changes in the horizontal temperature advection over the leeward side of LULCC regions in East Asia, Europe, and North America. Correlation coefficients of 0.71, 0.63, 0.50, and 0.72 are calculated for the western North Pacific Ocean, Mediterranean Sea–North Africa, North America–Atlantic Ocean, and eastern Pacific Ocean regions, respectively. All of these correlation coefficients can reach a significance level of

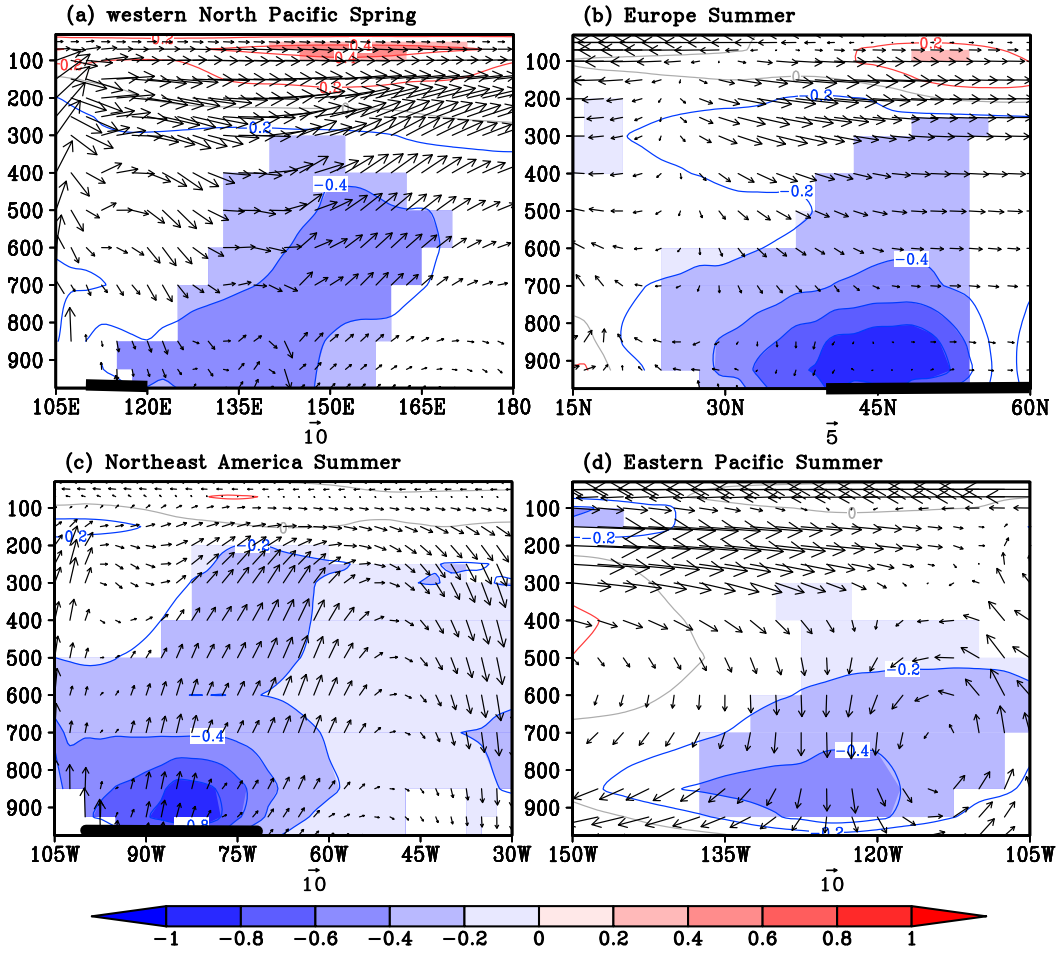

Figure 6. LULCC-induced change in air temperature and climatological-mean wind vector (the vertical wind multiplied by 100) averaged in (a) the western North Pacific (30°–40°N), (b) Europe (0°–40°E), (c) northeast North America (30°–45°N), and (d) eastern Pacific (20°–40°N) in different seasons. The shaded area indicates that the difference in the air temperature between the CurVeg and PotVeg experiments reaches the significance level of 0.05. The heavy line indicates the regions where LULCC occurs.

0.01. All regression slopes are positive, and a larger regression slope corresponds to a higher correlation coefficient. Given their high correlation coefficients, temperature advection likely plays a more important role in determining the changes in 850-hPa air temperatures in the western North Pacific Ocean and eastern Pacific Ocean regions than in the other two regions.

4.3. Changes in the vertical air temperature profile

To investigate the response of the upper air temperature to LULCC, we compute the LULCC-induced changes in the air temperature as a function of pressure

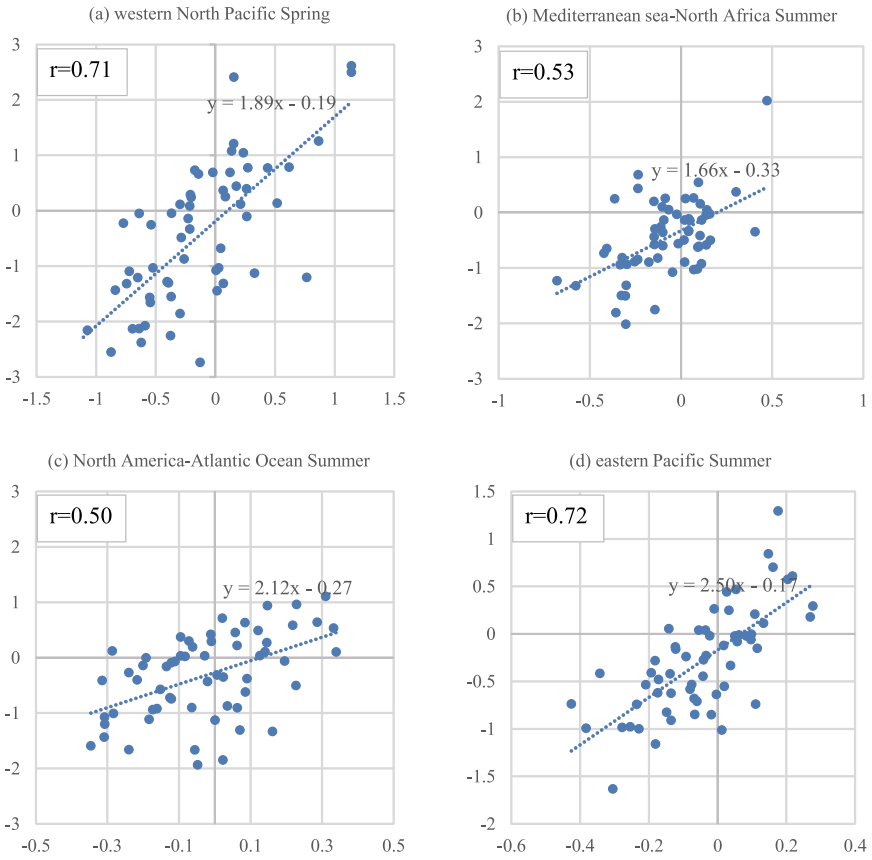

Figure 7. LULCC-induced changes in the 850-hPa horizontal advection of air temperature and 850-hPa air temperature (a) in the western North Pacific (30°–45°N, 120°–160°E) in spring, (b) in the Mediterranean Sea and North Africa region (25°–40°N, 20°W–40°E) in summer, (c) in North America and the Atlantic Ocean (45°–50°N, 20°–80°W) in summer, and (d) in the eastern Pacific (20°–40°N, 100°–160°W) in summer. The horizontal coordinate is the change of the 850-hPa horizontal advection and the unit is K day^{-1}; the vertical ordinate is the change of the 850-hPa air temperature, and the unit is in kelvins.

(Figure 8). An overall decrease in the global-mean air temperature is found throughout the troposphere with the maximum decrease of 0.1°C occurring in summer (Figure 8a). The air temperature averaged over the global land area shows a larger change than the global mean. The temperature change at the significance level of 0.1 extends upward and reaches 300 hPa in summer (Figure 8b). In general, cooling is more significant in the lower troposphere than in the upper troposphere, and the strongest cooling of −0.18°C occurs at 850 hPa in summer. The tropospheric-mean air temperature decreases by 0.13°C in summer and reaches the significance level of 0.05, although the changes in each individual level cannot always reach the same significance level (Table 4).

At the regional scale, LULCC-induced changes in air temperature are generally larger than the global means and appear to be season and region dependent (Figures 8, 9). For example, in East Asia, LULCC leads to a 0.2°–0.4°C decrease in air

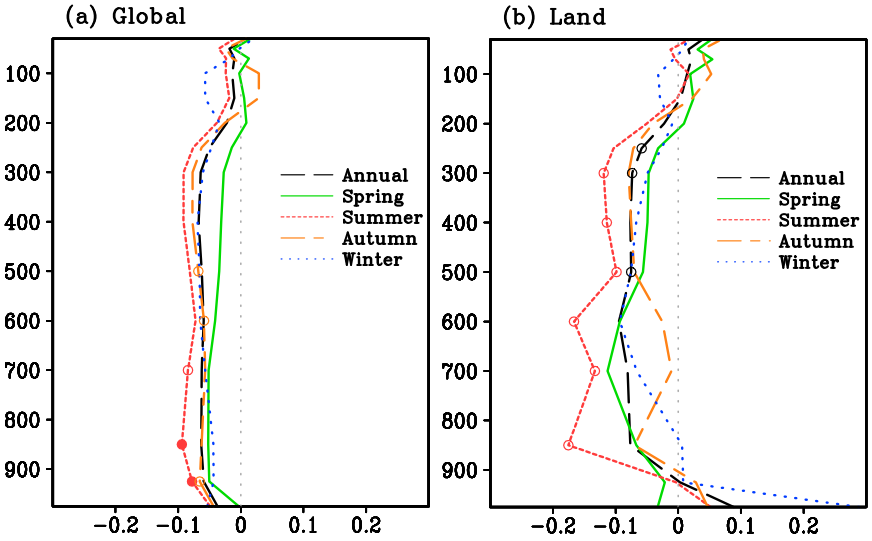

Figure 8. LULCC-induced changes in air temperature (a) over global and (b) over land area. Solid and open circles indicate that the difference between the CurVeg and PotVeg experiments reaches the significance levels of 0.05 and 0.1, respectively.

temperature between 700 and 300 hPa with significant decreases in the upper troposphere in spring and autumn. Conversely, changes in the air temperature over the same region are small in summer and winter and cannot reach the significance level of 0.1 between 700 and 200 hPa. The maximum decrease in the upper troposphere temperature in East Asia is likely related to the decrease in the latent heat release caused by the reduced precipitation in spring and autumn (Figure 9a; Table 3). The decrease of precipitation is 0.37 (0.28) mm day^{-1} in spring (autumn) but only 0.07 (0.12) mm day^{-1} in summer (winter). To illustrate the detailed changes in the vertical profile of the atmospheric heating rate, we computed the sum of the heating terms: the net shortwave and longwave heating rate, the heating due to the moist convective processes, and the heating due to vertical temperature diffusion parameterizations (Figure 10). The heating profiles also show similar changes as the temperature profiles (Figures 9, 10), suggesting that the tropospheric cooling likely resulted from the decreases in atmospheric heating rate. At lower troposphere, the decrease of air temperature is mainly caused by the vertical temperature diffusion. In contrast, the moist processes show significant decrease at the upper troposphere, which likely accounts for the upper-tropospheric cooling (not shown). The atmospheric heating rate shows a larger cooling in East Asia in spring and autumn relative to summer and winter, which is consistent with the changes in precipitation (Figure 10a; Table 3). It should be noted that the precipitation and atmospheric heating rate show more significant decreases in spring relative to autumn; however, the upper air temperature shows a larger decrease in autumn than in spring. This result is partly related to the climatological-mean wind speed. The upper wind speed is greater in spring than in autumn in East Asia (not shown). The larger wind speed tends to reduce the upper air cooling caused by the decrease in the atmospheric heating via stronger temperature

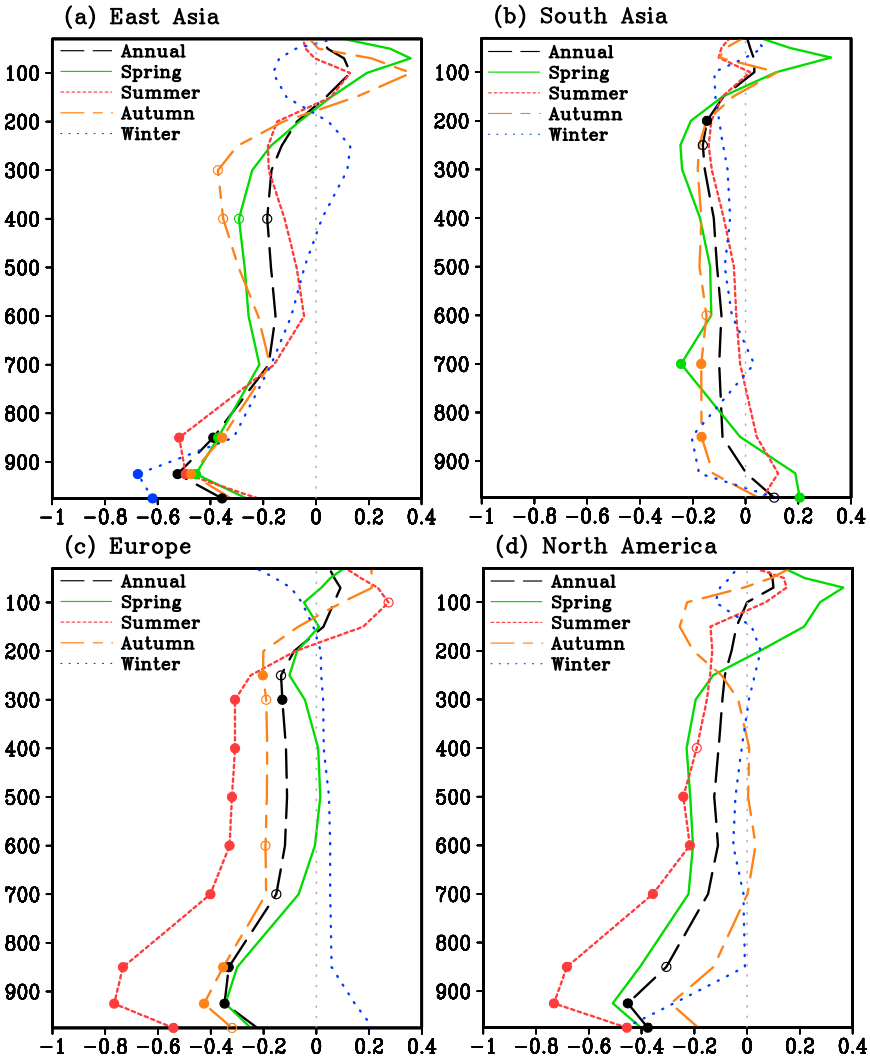

Figure 9. LULCC-induced changes in air temperature over global and over land area for (a) East Asia (25°–40°N, 110°–120°E), (b) South Asia (10°–30°N, 70°–90°E), (c) Europe (40°–60°N, 0°–40°E), and (d) North America (30°–45°N, 70°–100°W), respectively. Solid and open circles indicate that the difference between the CurVeg and PotVeg experiments reaches the significance levels of 0.05 and 0.1, respectively.

advection. As a result, the decrease in the upper air temperature in East Asia in spring is smaller than that in autumn. In addition, LULCC leads to a divergence and subsidence anomalies due to the reduced land surface roughness in East Asia and a decrease in the atmospheric moisture content. A decrease in the atmosphere moisture content leads to further decreases in the air temperature due to the greenhouse effect of water vapor. The positive feedback between the decreases in air temperature, the abnormal subsidence, and the reduced atmospheric moisture content can be maintained and eventually results in distinct decreases in precipitation (Xu et al. 2015). As

Table 3. LULCC-induced changes in precipitation (mm day^{-1}) averaged over land areas of East Asia (25°–40°N, 110°–120°E), South Asia (10°–30°N, 70°–90°E), Europe (40°–60°N, 0°–40°E), North America (30°–45°N, 70°–100°W), and global mean. Statistical significance alpha levels: [a] indicates 0.10 and [b] indicates 0.05.

	Spring	Summer	Autumn	Winter	Annual
East Asia	−0.37[b]	−0.07	−0.28	−0.12	−0.21[b]
South Asia	−0.20[a]	−0.19	−0.38	−0.13	−0.23[a]
Europe	−0.02	0.08[a]	−0.00	−0.07	−0.00
North America	0.03	−0.01	0.02	−0.05	−0.00
Global mean	−0.00	0.01	0.01	−0.01	0.00

shown in Figure 11, the specific humidity exhibits larger decrease in autumn compared to spring throughout the troposphere in East Asia, indicating that the positive feedback appears to be stronger in autumn than in spring. In South Asia, the changes in air temperature between 700 and 200 hPa are also larger in spring and autumn than in summer and winter, although the magnitudes of the decreases are smaller than those in East Asia (Figure 9b).

In Europe and North America, the most significant change in air temperature occurs in summer rather than in spring or autumn (Figures 9c,d). LULCC leads to a significant decrease in air temperature throughout the troposphere below 300 hPa (400 hPa) in Europe (North America) with the largest decrease of approximately 0.8°C occurring at 925 hPa in summer. The vertical temperature diffusion shows its maximum decrease at lower troposphere in summer in East Asia, Europe, and North America (not shown), which accounts for the low-level cooling of the atmosphere. The largest decrease in the air temperature, which occurs in summer in Europe and North America, is likely related to changes in the land–atmospheric energy budget. LULCC generally leads to significant decreases in both the ASR at the land surface and the SH (Figure 4). The decreases in ASR and SH favor the cooling of the atmosphere. The largest decreases in ASR and SH occur in summer in Europe and North America. Wind speed is also relatively weak in summer (not shown); thus, the influence of LULCC can be accumulated and helps to maintain low-level cooling. As a result, the tropospheric air temperature shows its largest decrease in summer. The changes in ASR and SH have stronger influences on the air temperature in the lower troposphere than in the upper troposphere. It is noted that the LULCC-induced increases in the land surface albedo is smaller in summer than in the other seasons in Europe and North America (Table 2). However, the largest decrease in ASR still occurs in summer because the insolation is stronger in summer than the other seasons. Europe is located at high latitudes, where solar insolation has a stronger annual cycle than in lower latitudes. Summer is also the dry season with less cloud cover in Europe, which allows more solar radiation to reach the land surface. Thus, ASR still shows maximum decrease although the change in land surface albedo is small in summer.

To quantify the influence of LULCC on the upper air temperature, we compute the changes in the tropospheric-mean air temperature induced by LULCC (Table 4). Although the LULCC-induced changes in the global-mean tropospheric temperature appear to be small, they can still reach the significance levels of 0.05 and 0.01 in the summer and autumn, respectively (Table 4). Changes in the air temperature in the four typical regions with significant LULCC are shown to be significantly larger than that

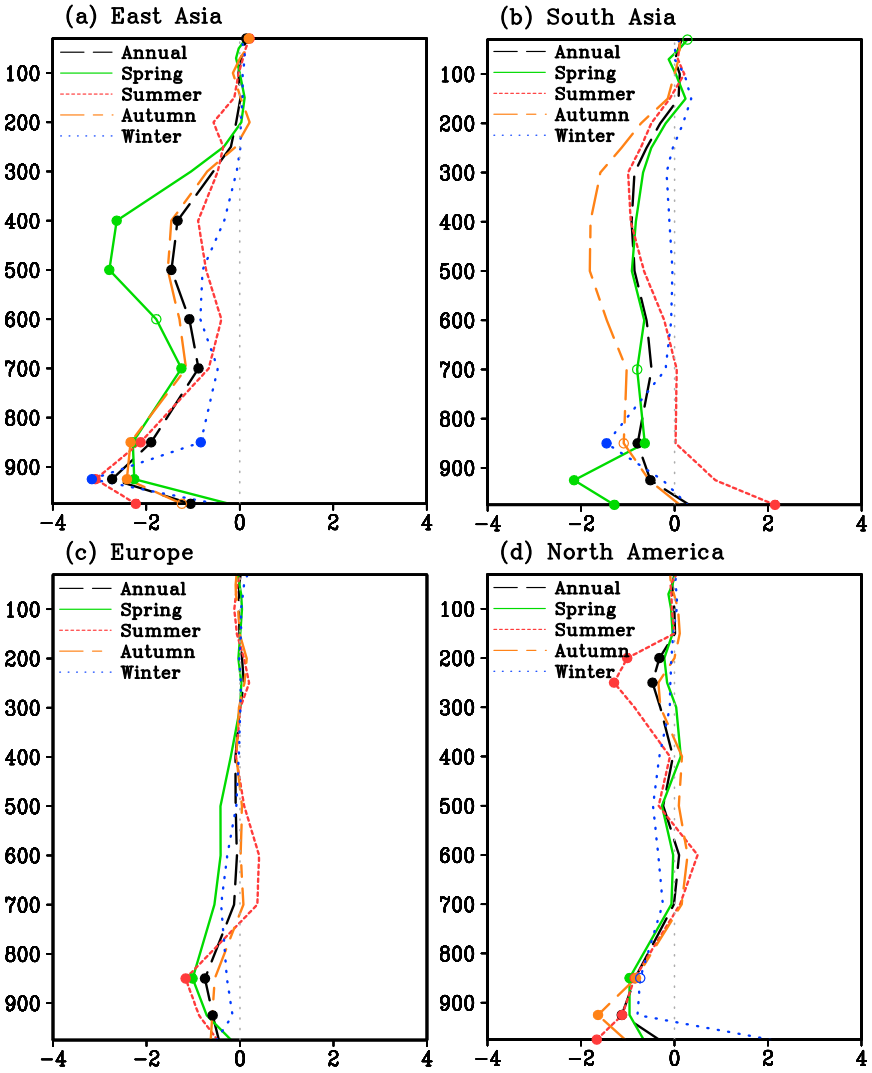

Figure 10. LULCC-induced changes in the sum of solar heating rate, longwave heating rate, vertical temperature diffusion and temperature tendency moist processes (10^{-6} K s^{-1}) in East Asia (25°–40°N, 110°–120°E), South Asia (10°–30°N, 70°–90°E), Europe (40°–60°N, 0°–40°E), and North America (30°–45°N, 70°–100°W). Solid and open circles indicate that the difference between the CurVeg and PotVeg experiments reaches the significance levels of 0.05 and 0.1, respectively.

of the global-mean temperature. The changes in the regional air temperatures in East Asia, South Asia, Europe, and North America can be 2 to 3 times larger than the global mean (Table 4). In monsoon regions (i.e., East Asia and South Asia), the changes in tropospheric air temperatures are larger in spring and autumn than in summer and winter. In East Asia, the tropospheric-mean air temperature decreases by 0.24°C in spring and 0.28°C in autumn, while the decrease is 0.21°C in summer and 0.12°C in winter (Table 4). Similar to East Asia, the decrease in tropospheric air temperature is

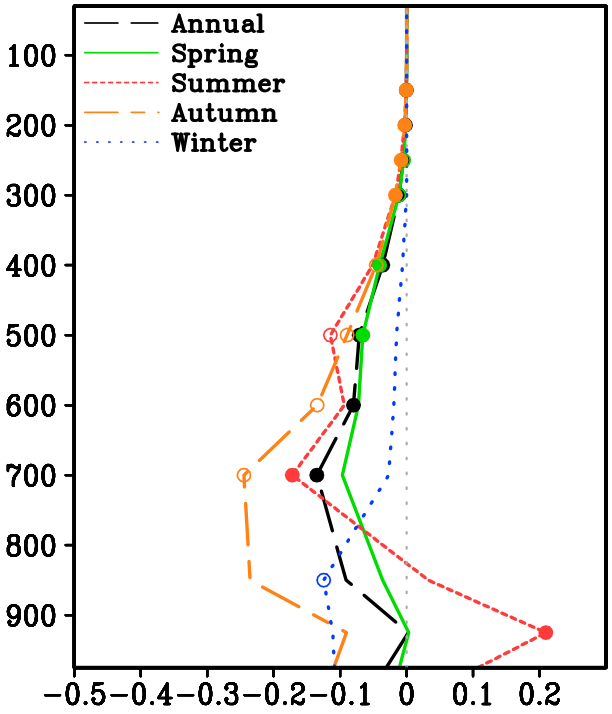

Figure 11. LULCC-induced changes in specific humidity (g kg^{-1}) in East Asia (25°–40°N, 110°–120°E). Solid and open circles indicate that the difference between the CurVeg and PotVeg experiments reaches the significance levels of 0.05 and 0.1, respectively.

also the largest in spring and autumn in South Asia. Conversely, the tropospheric-mean air temperature decreases significantly by 0.42° and 0.36°C in summer in Europe and North America, respectively (Table 4). Clearly, LULCC can lead to detectable changes in tropospheric air temperatures in addition to the changes in the LST.

5. Conclusions

In this study, we examined the possible responses of the surface and upper air temperatures to LULCC and their seasonality using the fully coupled Community

Table 4. LULCC-induced changes in the mass-weighted tropospheric-mean air temperature between surface and 200-hPa averaged over land areas of East Asia (25°–40°N, 110°–120°E), South Asia (10°–30°N, 70°–90°E), Europe (40°–60°N, 0°–40°E), North America (30°–45°N, 70°–100°W), and global mean. Statistical significance alpha levels: [a] indicates 0.10, and [b] indicates 0.05.

	Spring	Summer	Autumn	Winter	Annual
East Asia	−0.24	−0.21	−0.28[b]	−0.12	−0.21[b]
South Asia	−0.16	0.03	−0.15	−0.08	−0.09
Europe	−0.20	−0.42[b]	−0.20	0.24	−0.15[a]
North America	−0.27	−0.36[b]	−0.06	0.02	−0.17
Global mean	−0.07	−0.13[b]	−0.07[a]	−0.04	−0.08[a]

Earth System Model (CESM). The primary conclusions of this study are briefly summarized below.

Model results indicate that LULCC can lead to significant increases in the LST by approximately 1°– 3°C in South Asia and 1°C in East Asia throughout the year. Conversely, LULCC can also lead to year-round significant decreases in LST in North America and North Africa except in spring. These changes in the LST are closely related to LULCC-induced changes in the land surface albedo, roughness length, sensible heat flux, and latent heat flux. In East Asia, the increase in the LST is primarily attributed to the reduced sensible heat flux. Conversely, hydrological processes play a more important role in South Asia. In Europe and North America, ASR decreases due to the increase in the surface albedo, which favors the land surface cooling. However, the significant decrease in SH tends to warm the land surface, which largely cancels out the cooling effect induced by the albedo change (Figure 4). As a result, the cooling is weak in Europe and North America. In North Africa, where no clear LULCC occurs, LST still shows a significant decrease due to an enhanced cold advection from Europe to North Africa.

Compared with changes in the LST, the response of the upper air temperature to LULCC is less region dependent and is characterized by an overall cooling at 850 hPa in LULCC regions and in their leeward regions. LULCC leads to decreases in the surface roughness, sensible heat flux, and latent heat flux; these decreases tend to warm the land surface but cool the upper atmosphere. However, the increase in land surface albedo is favorable for the cooling of both the land surface and troposphere. At the global scale, LULCC leads to a weak decrease in the tropospheric-mean air temperature by 0.08°C annually. At the regional scale, changes in the tropospheric air temperature can be 2 to 3 times larger than the global-mean temperature. In East Asia and South Asia, the upper-tropospheric temperature shows a decrease of 0.24°C (0.28°C) in spring (autumn), which is primarily due to the decrease in the latent heat release from precipitation. Similar to East Asia, the tropospheric-mean air temperature also shows large decreases of 0.16° and 0.15°C in spring and autumn in South Asia, respectively. Conversely, LULCC leads to the maximum decreases in tropospheric-mean temperature (e.g., 0.42° and 0.36°C) in Europe and North America, respectively, in summer. Different from monsoon regions, most significant cooling occurs in summer in Europe and North America due to the greatest decreases in absorbed solar radiation and sensible heat flux.

In addition to local responses to LULCC, nonlocal responses of upper air temperature to LULCC can also be found in the model results. There is a significant decrease in 850-hPa air temperatures over the leeward sides of LULCC regions, including the western North Pacific, the Mediterranean Sea, North Africa, the eastern Pacific Ocean, and the northwestern Atlantic Ocean. The 850-hPa air temperature decreases by 0.4°–0.6°C in the western North Pacific in spring due to the enhanced cold advection from East Asia. Similarly, the 850-hPa air temperature decreases by approximately 0.4°, 0.6°, and 0.4°C in summer in the Mediterranean Sea and North Africa region, the eastern Pacific Ocean, and the North America and Atlantic Ocean region, respectively, which can also be attributed to the LULCC-induced changes in the horizontal temperature advection.

It should be noted that the results of this study are solely based on simulations of a single Earth system model; different models may show different sensitivities to

the LULCC. Thus, the results reported in this study are likely model dependent. In addition, the model used in this study contained significant systematic errors that could affect the conclusions in this study. Therefore, multimodel ensemble simulations would help to validate the influence of LULCC on tropospheric air temperature and warrant further studies.

Acknowledgments. This research is jointly sponsored by the ''National Basic Research Program of China'' (2011CB952004), Key Technologies R&D Program of China (Grant 2012BAC22B04), National Natural Science Foundation of China (Grants 41475063, 40905042), and Program for New Century Excellent Talents in University.

References

Abe, M., A. Kitoh, and T. Yasunari, 2003: An evolution of the Asian summer monsoon associated with mountain uplift—Simulation with the MRI atmosphere-ocean coupled GCM. *J. Meteor. Soc. Japan*, **81**, 909–933, doi:10.2151/jmsj.81.909.

Bala, G., K. Caldeira, M. Wickett, T. J. Phillips, D. B. Lobell, C. Delire, and A. Mirin, 2007: Combined climate and carbon-cycle effects of large-scale deforestation. *Proc. Natl. Acad. Sci. USA*, **104**, 6550–6555, doi:10.1073/pnas.0608998104.

Betts, R. A., P. D. Falloon, K. K. Goldewijk, and N. Ramankutty, 2007: Biogeophysical effects of land use on climate: Model simulations of radiative forcing and large-scale temperature change. *Agric. For. Meteor.*, **142**, 216–233, doi:10.1016/j.agrformet.2006.08.021.

Bitz, C. M., M. Holland, M. Eby, and A. J. Weaver, 2001: Simulating the ice-thickness distribution in a coupled climate model. *J. Geophys. Res.*, **106**, 2441–2463, doi:10.1029/1999JC000113.

Bonan, G. B., 2008: Forests and climate change: Forcings, feedbacks, and the climate benefits of forests. *Science*, **320**, 1444–1449, doi:10.1126/science.1155121.

Brovkin, V., A. Ganopolski, M. Claussen, C. Kubatzki, and V. Petoukhov, 1999: Modeling climate response to historical land cover change. *Global Ecol. Biogeogr.*, **8**, 509–517, doi:10.1046/j.1365-2699.1999.00169.x.

Chase, T. N., R. A. Pielke, T. G. F. Kittel, R. P. Nemani, and S. W. Running, 1996: Sensitivity of a general circulation model to global changes in leaf area index. *J. Geophys. Res.*, **101**, 7393–7408, doi:10.1029/95JD02417.

Collins, W. D., and Coauthors, 2006: The Community Climate System Model version 3 (CCSM3). *J. Climate*, **19**, 2122–2143, doi:10.1175/JCLI3761.1.

Dai, Y., and Coauthors, 2003: The Common Land Model. *Bull. Amer. Meteor. Soc.*, **84**, 1013–1023, doi:10.1175/BAMS-84-8-1013.

Davin, E. L., and N. de Noblet-Ducoudré, 2010: Climatic impact of global-scale deforestation: Radiative versus nonradiative processes. *J. Climate*, **23**, 97–112, doi:10.1175/2009JCLI3102.1.

de Noblet-Ducoudré, N., and Coauthors, 2012: Determining robust impacts of land-use-induced land cover changes on surface climate over North America and Eurasia: Results from the first set of LUCID experiments. *J. Climate*, **25**, 3261–3281, doi:10.1175/JCLI-D-11-00338.1.

Dickinson, R. E., and P. Kennedy, 1992: Impacts on regional climate of Amazon deforestation. *Geophys. Res. Lett.*, **19**, 1947–1950, doi:10.1029/92GL01905.

Douglas, E. M., D. Niyogi, S. Frolking, J. B. Yeluripati, R. A. Pielke Sr., N. Niyogi, C. J. Vörösmarty, and U. C. Mohanty, 2006: Changes in moisture and energy fluxes due to agricultural land use and irrigation in the Indian monsoon belt. *Geophys. Res. Lett.*, **33**, L14403, doi:10.1029/2006GL026550.

Feddema, J. J., K. W. Oleson, G. B. Bonan, L. O. Mearns, L. E. Buja, G. A. Meehl, and W. M. Washington, 2005: The importance of land-cover change in simulating future climates. *Science*, **310**, 1674–1678, doi:10.1126/science.1118160.

Findell, K. L., T. R. Knutson, and P. C. D. Milly, 2006: Weak simulated extratropical responses to complete tropical deforestation. *J. Climate*, **19**, 2835–2850, doi:10.1175/JCLI3737.1.

——, A. J. Pitman, M. H. England, and P. J. Pegion, 2009: Regional and global impacts of land cover change and sea surface temperature anomalies. *J. Climate*, **22**, 3248–3268, doi:10.1175/2008JCLI2580.1.

Fu, C., 2003: Potential impacts of human-induced land cover change on East Asia monsoon. *Global Planet. Change*, **37**, 219–229, doi:10.1016/S0921-8181(02)00207-2.

Haxeltine, A., and C. I. Prentice, 1996: BIOME3: An equilibrium terrestrial biosphere model based on ecophysiological constraints, resource availability, and competition among plant functional types. *Global Biogeochem. Cycles*, **10**, 693–709, doi:10.1029/96GB02344.

Hurtt, G. C., and Coauthors, 2006: The underpinnings of land-use history: Three centuries of global gridded land-use transitions, wood-harvest activity, and resulting secondary lands. *Global Change Biol.*, **12**, 1208–1229, doi:10.1111/j.1365-2486.2006.01150.x.

Kantha, L. H., and C. A. Clayson, Eds., 2000: *Numerical Models of Oceans and Oceanic Process*. International Geophysics Series, Vol. 66, Academic Press, 940 pp.

Kitoh, A., 2004: Effects of mountain uplift on East Asian summer climate investigated by a coupled atmosphere–ocean GCM. *J. Climate*, **17**, 783–802, doi:10.1175/1520-0442(2004)017<0783:EOMUOE>2.0.CO;2.

Lawrence, P. J., and T. N. Chase, 2010: Investigating the climate impacts of global land cover change in the community climate system model. *Int. J. Climatol.*, **30**, 2066–2087, doi:10.1002/joc.2061.

Lee, E., T. N. Chase, B. Rajagopalan, R. Barry, T. W. Biggs, and P. J. Lawrence, 2009: Effects of irrigation and vegetation activity on early Indian summer monsoon variability. *Int. J. Climatol.*, **29**, 573–581, doi:10.1002/joc.1721.

Lin, S. J., 2004: A ''vertically Lagrangian'' finite-volume dynamical core for global models. *Mon. Wea. Rev.*, **132**, 2293–2307, doi:10.1175/1520-0493(2004)132<2293:AVLFDC>2.0.CO;2.

Lipscomb, W. H., 2001: Remapping the thickness distribution in sea ice models. *J. Geophys. Res.*, **106**, 13 989–14 000, doi:10.1029/2000JC000518.

Lobell, D. B., G. Bala, and P. B. Duffy, 2006: Biogeophysical impacts of cropland management changes on climate. *Geophys. Res. Lett.*, **33**, L06708, doi:10.1029/2005GL025492.

Maynard, K., and J. F. Royer, 2004: Effects of ''realistic'' land-cover change on a greenhouse-warmed African climate. *Climate Dyn.*, **22**, 343–358, doi:10.1007/s00382-003-0371-z.

Meehl, G. A., J. M. Arblaster, D. M. Lawrence, A. Seth, E. K. Schneider, B. P. Kirtman, and D. Min, 2006: Monsoon regimes in the CCSM3. *J. Climate*, **19**, 2482–2495, doi:10.1175/JCLI3745.1.

——, ——, J. M. Caron, H. Annamalai, M. Jochum, A. Chakraborty, and R. Murtugudde, 2012: Monsoon regimes and processes in CCSM4. Part I: The Asian–Australian monsoon. *J. Climate*, **25**, 2583–2608, doi:10.1175/JCLI-D-11-00184.1.

Myhre, G., and Coauthors, 2013: Anthropogenic and natural radiative forcing. *Climate Change 2013: The Physical Science Basis*, T. F. Stocker et al., Eds., Cambridge University Press, 659–740.

Narisma, G. T., and A. J. Pitman, 2003: The impact of 200 years of land cover change on the Australian near-surface climate. *J. Hydrometeor.*, **4**, 424–436, doi:10.1175/1525-7541(2003)4<424:TIOYOL>2.0.CO;2.

Niyogi, D., Y. K. Xue, and S. Raman, 2002: Hydrological land surface response in a tropical regime and a midlatitudinal regime. *J. Hydrometeor.*, **3**, 39–56, doi:10.1175/1525-7541(2002)003<0039:HLSRIA>2.0.CO;2.

Oleson, K. W., G. B. Bonan, S. Levis, and M. Vertenstein, 2004: Effects of land use change on U.S. climate: Impact of surface datasets and model biogeophysics. *Climate Dyn.*, **23**, 117–132, doi:10.1007/s00382-004-0426-9.

Pielke, R. A., 2001: Influence of the spatial distribution of vegetation and soils on the prediction of cumulus convective rainfall. *Rev. Geophys.*, **39**, 151–177, doi:10.1029/1999RG000072.

——, G. Marland, R. A. Betts, T. N. Chase, J. L. Eastman, J. O. Niles, D. Niyogi, and S. W. Running, 2002: The influence of land-use change and landscape dynamics on the climate system: Relevance to climate-change policy beyond the radiative effect of greenhouse gases. *Philos. Trans. Roy. Soc. London*, **A360**, 1705–1719, doi:10.1098/rsta.2002.1027.

Pitman, A. J., and Coauthors, 2009: Uncertainties in climate responses to past land cover change: First results from the LUCID intercomparison study. *Geophys. Res. Lett.*, **36**, L14814, doi:10.1029/2009GL039076.

Polcher, J., and K. Laval, 1994: A statistical study of the regional impacts of deforestation on climate in the LMD GCM. *Climate Dyn.*, **10**, 205–219, doi:10.1007/BF00208988.

Ramankutty, N., and J. A. Foley, 1999: Estimating historical changes in global land cover: Croplands from 1700 to 1992. *Global Biogeochem. Cycles*, **13**, 997–1027, doi:10.1029/1999GB900046.

Schneck, R., and V. Mosbrugger, 2011: Simulated climate effects of Southeast Asian deforestation: Regional processes and teleconnection mechanisms. *J. Geophys. Res.*, **116**, D11116, doi:10.1029/2010JD015450.

Shukla, J., C. Nobre, and P. Sellers, 1990: Amazon deforestation and climate change. *Science*, **247**, 1322–1325, doi:10.1126/science.247.4948.1322.

Smith, R. D., and Coauthors, 2010: The Parallel Ocean Program (POP) reference manual. Los Alamos National Laboratory Tech. Rep. LAUR-10-01853, 140 pp.

Snyder, P. K., 2010: The influence of tropical deforestation on the Northern Hemisphere climate by atmospheric teleconnections. *Earth Interact.*, **14**, doi:10.1175/2010EI280.1.

Wohlfahrt, J., S. P. Harrison, and P. Braconnot, 2004: Synergistic feedbacks between ocean and vegetation on mid- and high-latitude climates during the mid-Holocene. *Climate Dyn.*, **22**, 223–238, doi:10.1007/s00382-003-0379-4.

Xu, Z., R. Mahmood, Z. L. Yang, C. Fu, and H. Su, 2015: Investigating diurnal and seasonal climatic response to land use and land cover change over monsoon Asia with the Community Earth System Model. *J. Geophys. Res. Atmos.*, **120**, 1137–1152, doi:10.1002/2014JD022479.

Zhang, H., A. Henderson-Sellers, and K. McGuffie, 1996: Impacts of tropical deforestation. Part I: Process analysis of local climatic change. *J. Climate*, **9**, 1497–1517, doi:10.1175/1520-0442(1996)009<1497:IOTDPI>2.0.CO;2.

Zhao, M., A. J. Pitman, and T. N. Chase, 2001: The impact of land cover change on the atmospheric circulation. *Climate Dyn.*, **17**, 467–477, doi:10.1007/PL00013740.

Zwiers, F. Z., and H. von Storch, 1995: Taking serial correlation into account in tests of the mean. *J. Climate*, **8**, 336–351, doi:10.1175/1520-0442(1995)008<0336:TSCIAI>2.0.CO;2.